Chinese Journal of
POLYMER SCIENCE

RESEARCH ARTICLE

https://doi.org/10.1007/s10118-022-2673-9
Chinese J. Polym. Sci. **2022**, *40*, 248–255

Thermally Conductive Poly(lactic acid) Composites with Superior Electromagnetic Shielding Performances *via* 3D Printing Technology

Teng-Bo Ma[a], Hao Ma[a], Kun-Peng Ruan[a], Xue-Tao Shi[a*], Hua Qiu[a,b], Sheng-Yuan Gao[a], and Jun-Wei Gu[a*]

[a] *Shaanxi Key Laboratory of Macromolecular Science and Technology, School of Chemistry and Chemical Engineering, Northwestern Polytechnical University, Xi'an 710072, China*
[b] *School of Materials Science and Engineering, Henan University of Science and Technology, Luoyang 471023, China*

Electronic Supplementary Information

Abstract This work proposes a facile fabrication strategy for thermally conductive graphite nanosheets/poly(lactic acid) sheets with ordered GNPs (o-GNPs/PLA) *via* fused deposition modeling (FDM) 3D printing technology. Further combinations of o-GNPs/PLA with $Ti_3C_2T_x$ films prepared by vacuum-assisted filtration were carried out by "layer-by-layer stacking-hot pressing" to be the thermally conductive $Ti_3C_2T_x$/(o-GNPs/PLA) composites with superior electromagnetic interference shielding effectiveness (EMI SE). When the content of GNPs was 18.60 wt% and 4 layers of $Ti_3C_2T_x$ (6.98 wt%) films were embedded, the in-plane thermal conductivity coefficient ($\lambda_{||}$) and EMI SE (EMI $SE_{||}$) values of the thermally conductive $Ti_3C_2T_x$/(o-GNPs/PLA) composites significantly increased to 3.44 $W{\cdot}m^{-1}{\cdot}K^{-1}$ and 65 dB (3.00 mm), increased by 1223.1% and 2066.7%, respectively, compared with $\lambda_{||}$ (0.26 $W{\cdot}m^{-1}{\cdot}K^{-1}$) and EMI $SE_{||}$ (3 dB) of neat PLA matrix. This work offers a novel and easily route for designing and manufacturing highly thermally conductive polymer composites with superior EMI SE for broader application.

Keywords Polymer-matrix composites (PMCs); $Ti_3C_2T_x$; 3D printing; Thermal conductivity; Electromagnetic interference (EMI)

Citation: Ma, T. B.; Ma, H.; Ruan, K. P.; Shi, X. T.; Qiu, H.; Gao, S. Y.; Gu, J. W. Thermally conductive poly(lactic acid) composites with superior electromagnetic shielding performances *via* 3D printing technology. *Chinese J. Polym. Sci.* **2022**, *40*, 248–255.

INTRODUCTION

With the booming development of high-frequency, high-power and high-density electronic system and components, the resulted serious heat dissipation problems restrict the stability, reliability and service life of electronic equipment and devices.[1,2] Meantime, with the rapid development of the fifth generation (5G) communication technology, the problems of electromagnetic radiation pollution and information security are becoming more and more prominent.[3–5] Simultaneously, part of the electromagnetic radiation absorbed by materials will also be converted into heat, which would further aggravate the heat accumulation and seriously threaten the safety of equipment and consumers.[6,7]

Polymer-matrix composites play irreplaceable role in the fields of electronic instruments and telecommunication equipment due to their advantages such as lightweight, excellent specific strength, easy processibility and good corrosion resistance, *etc.*[8–10] However, the intrinsic thermal conductivity coefficient (λ) of the polymer matrix are relatively low (0.18–0.44 $W{\cdot}m^{-1}{\cdot}K^{-1}$), hardly to satisfy the requirements of efficient heat conduction/dissipation of electronic products. At present, the traditional solution is to directly introduce highly thermally conductive fillers (such as boron nitride nanosheets (BNNSs),[11,12] aluminum nitride (AlN),[13,14] silicon carbide (SiC),[15,16] carbon nanotubes (CNTs),[17–20] graphene,[21–25] *etc.*) into polymer matrix. This method presents simple procedure and is widely used in practical industrial production. Traditionally, the thermally conductive fillers are randomly distributed inner polymer matrix, and a high filling amount is required to build up efficient thermally conductive networks inner polymer matrix in order to obtain relatively higher λ. However, high content of thermally conductive fillers not only leads to more "filler-filler" and "filler-polymer" interfacial thermal barriers, which is unfavorable to the improvement of thermal conductivity, but also results in problems such as processing difficulty and deterioration of entire mechanical properties.[26–28]

Targeting to the above-mentioned problems, researchers reported strategies such as the prefabricated thermal conductive networks,[29] and electrospinning[30] methods, aiming to promote the ordered arrangement of thermally conductive fillers inner polymer matrix effectively, so as to improve the construction efficiency of the thermally conductive net-

* Corresponding authors, E-mail: shixuetao@nwpu.edu.cn (X.T.S.)
E-mail: gjw@nwpu.edu.cn; nwpugjw@163.com (J.W.G.)

Invited Research Article for the 40th Anniversary of *Chinese Journal of Polymer Science*
Received October 25, 2021; Accepted November 29, 2021; Published online January 12, 2022

works, and thereby improving λ values of the polymer composites. Hu *et al.*[31] prefabricated three-dimensional BN (3D-BN) thermally conductive networks *via* ice template self-assembly, followed by infiltration and curing of epoxy resin to obtain the thermally conductive 3D-BN/epoxy composites. When the content of BN is 34 vol%, the λ of the thermally conductive 3D-BN/epoxy composites is 4.42 $W{\cdot}m^{-1}{\cdot}K^{-1}$, 281.0% higher than that of the thermally conductive BN/epoxy composites with random BN dispersion. This great improvement of λ is mainly due to the ordered arrangement of BN in the thermally conductive 3D-BN/epoxy composites, which is more favorable for constructing BN thermally conductive networks. Yang *et al.*[32] prepared BNNSs/CNTs/PVA fiber network with oriented BNNSs/CNTs hybrid fillers by electrospinning, and then obtained the thermally conductive (BNNSs/CNTs)/epoxy composites after following impregnation and curing of epoxy resin. When the amount of BNNSs/CNTs hybrid fillers is 27.5 wt% (CNTs 0.35 wt%), the in-plane λ ($\lambda_{||}$) of the thermally conductive (BNNSs/CNTs)/epoxy composites can reach 6.3 $W{\cdot}m^{-1}{\cdot}K^{-1}$, which is about 88% higher than that of the thermally conductive (BNNSs-70)/epoxy composites (3.4 $W{\cdot}m^{-1}{\cdot}K^{-1}$) without CNTs, mainly due to the easier construction of thermally conductive BNNSs/CNTs networks by electrospinning. In our former work, the strategy of "electrospinning-hot pressing" was proposed to prepare thermally conductive polymer composites, which effectively achieved the ordered arrangement and efficient lapping of thermally conductive fillers inner polymer matrix, further improving the thermal conductivities of the composites.[33–36] For example, when the amount of BNNSs is 30 wt%, the $\lambda_{||}$ of thermally conductive BNNSs/PVA composite film by electrospinning is as high as 18.63 $W{\cdot}m^{-1}{\cdot}K^{-1}$, 32.1 times that of BNNSs/PVA composites film (0.58 $W{\cdot}m^{-1}{\cdot}K^{-1}$) prepared by traditional blending method.[37] Even the above methods effectively promote the construction of thermally conductive pathway inner polymer composites, there are still some drawbacks, such as complex process, long production cycle or requirement of expensive production equipment.

3D printing technology features specially in designing and preparing complex shapes and structures that are hard to be manufactured by traditional technologies, which has been widely used in aerospace,[38] automobile,[39] environment,[40] medicine,[41] wearable devices[42] and other fields. Compared with selective laser sintering (SLS), stereo lithography apparatus (SLA) and digital light procession (DLP), fused deposition modeling (FDM) 3D printing technologies possess the advantages such as simple preparation process, short production cycle and cheaper production equipment.[43–46] Gnanasekaran *et al.*[47] prepared GNPs/PLA electromagnetic shielding composites by FDM 3D printing. The obtained EMI SE value of the GNPs/PLA composites with 12 wt% GNPs was 10 dB at 30 GHz, higher than that of the blend processed GNPs/PLA composites with the same GNPs content. What's more, FDM 3D printing technology has been reported to achieve the orderly arrangement of fillers and the construction of filler networks more conveniently and efficiently, due to the melt flow orientation in the process of polymer extrusion.[48,49] Jing *et al.*[50] reported the melting blend of linear low density polyethylene (LLDPE) with graphite nanosheets (GNPs) firstly into filaments, followed by FDM 3D printing into GNPs/LLDPE composites. When the content of GNPs is 15 vol%, the λ of EDF printed GNPs/LLDPE composites along the printing filament direction is 3.43 $W{\cdot}m^{-1}{\cdot}K^{-1}$, much higher than that of GNPs/LLDPE composites (1.98 $W{\cdot}m^{-1}{\cdot}K^{-1}$) prepared by molding with the same amount of GNPs. In addition, FDM 3D printing technology can endow the materials with strong designability, and to achieve the regulation of the internal microstructures of the composites by topology design, facilitating multiple reflections of electromagnetic waves inner electromagnetic shielding composites and the consequential improvement of EMI SE.[51–53] Wang *et al.*[54] used FDM 3D printing technology to construct porous PLA skeleton, which was impregnated into CNTs aqueous solution to prepare porous CNTs/PLA. Then the fabricated electromagnetic shielding 3D-CNTs/PLA composites with isolation structure were prepared by thermal molding. When the content of 3D-CNTs is 2 wt%, the EMI SE of electromagnetic shielding 3D CNTs/PLA composites at X-band is 40 dB, 20 dB higher than that of SM-CNTs/PLA composites (20 dB) prepared by blending molding with the same content of CNTs. Therefore, FDM 3D printing technology can facilitate the overlapping of fillers and efficient construction of network inner polymer composites, and would be considered as an efficient and simple strategy for preparing polymer composites with high thermal conductivity and excellent EMI SE.

In this work, o-GNPs/PLA sheets with orderly arrangement of GNPs fillers were prepared by FDM 3D printing technology with PLA as polymer matrix and GNPs as thermally conductive fillers. The thermally conductive $Ti_3C_2T_x$/(o-GNPs/PLA) composites with superior EMI SE were further prepared by "layer-by-layer stacking-hot pressing" process, with introducing $Ti_3C_2T_x$ films prepared by vacuum-assisted filtration. Morphologies of the thermally conductive GNPs/PLA composites were characterized by scanning electron microscope (SEM). Chemical structures and morphologies of the $Ti_3C_2T_x$ films were characterized by X-ray diffraction (XRD), X-ray photoelectron spectroscopy (XPS), SEM and atomic force microscope (AFM). The GNPs arrangement and dosage affecting on the thermal conductivities of the thermally conductive GNPs/PLA composites were investigated. Furthermore, the effects of the layer number of $Ti_3C_2T_x$ films on the related thermal conductivities, electrical conductivities, electromagnetic shielding performances and thermal properties of the thermally conductive $Ti_3C_2T_x$/(o-GNPs/PLA) composites were also studied.

EXPERIMENTAL

Fabrication of the Thermally Conductive GNPs/PLA Composites

Dried PLA pallets were compounded with GNPs powder by melting extrusion. The corresponding temperatures of feeding section, melting section and extrusion section were set up to be 30, 140 and 125 °C, respectively. By controlling the extrusion speed and the pulling rate with the die diameter of 2 mm, the related GNPs/PLA filament with a diameter of 1.75 mm was extruded. Then, the prepared GNPs/PLA filament was installed in a 3D printer (CreatBot F160) to prepare the thermally conductive o-GNPs/PLA composites. In this work, the print

https://doi.org/10.1007/s10118-022-2673-9

nozzle diameter and the layer height were fixed to be 0.4 and 0.2 mm, with the printing temperature to be 190 °C, and the filling density to be 100%. In addition, the thermally conductive GNPs/PLA composites were also prepared by hot pressing GNPs/PLA premix at 190 °C as referenced samples and marked as r-GNPs/PLA. The corresponding preparation processes of the o-GNPs/PLA and r-GNPs/PLA composites are shown in Fig. 1.

Fabrication of the Thermally Conductive $Ti_3C_2T_x$/(o-GNPs/PLA) Composites

According to our former work,[55,56] $Ti_3C_2T_x$ nanosheets were prepared based on the minimally intensive layer delamination (MILD) method. $Ti_3C_2T_x$ films prepared by vacuum assisted filtration, were immersed in dichloromethane solution with PLA concentration of 0.05 g/mL, and then placed in fume hood until the completely evaporation of the solvent. The treated $Ti_3C_2T_x$ films and o-GNPs/PLA sheets were laid alternately in the preheated 170°C mold under pressure of 10 MPa for 5 min. Then, the layered samples were demolded after natural cooling to obtain the thermally conductive $Ti_3C_2T_x$/(o-GNPs/PLA) composites (see Fig. S1 in the electronic supplementary information, ESI). The thermally comductive $Ti_3C_2T_x$/(o-GNPs/PLA) composites with n layers of $Ti_3C_2T_x$ films were marked as $Ti_3C_2T_x$-n/(o-GNPs/PLA) (n=0, 1, 2, 4) and their corresponding compositions were listed in Table S1 (in ESI).

The information of "**Materials**" and "**Characterizations**" were detailed in ESI.

RESULTS AND DISCUSSION

Thermally Conductive GNPs/PLA Composites

Fig. 2 shows the in-plane λ ($\lambda_{\parallel}$, Fig. 2a) and cross-plane λ ($\lambda_{\perp}$, Fig. 2b) values of the thermally conductive GNPs/PLA composites and the corresponding SEM photographs (Fig. 2c and Fig. 2d). The $\lambda_{\parallel}$ values of the r-GNPs/PLA and o-GNPs/PLA composites increase with the increase of GNPs content. With the same GNPs content, the $\lambda_{\parallel}$ values of o-GNPs/PLA composites are significantly higher than those of r-GNPs/PLA composites. When the loading of GNPs is 30 wt%, the $\lambda_{\parallel}$ of o-GNPs/PLA composites is 3.93 $W{\cdot}m^{-1}{\cdot}K^{-1}$, 1.5 times that of r-GNPs/PLA (2.55 $W{\cdot}m^{-1}{\cdot}K^{-1}$) with the same loading of GNPs, and 15.1 times that of neat PLA (0.26 $W{\cdot}m^{-1}{\cdot}K^{-1}$). With the increase of GNPs content, the increased $\lambda_{\parallel}$ vaues of the GNPs/PLA composites are due to the enhanced possibility of GNPs-GNPs thermally conductive pathway inner PLA matrix. In addition, more closely arranged filaments are presented in 3D printed o-GNPs/PLA composites following the in-plane direction achieved by FDM technique (Fig. 2c), resulting in more GNPs-GNPs thermally conductive pathway in the in-plane direction. Therefore, higher $\lambda_{\parallel}$ values were achieved in o-GNPs/PLA composites. With the same loading of GNPs, the $\lambda_{\perp}$ values of the o-GNPs/PLA composites are markedly lower than those of the r-GNPs/PLA composites (Fig. 2b). The $\lambda_{\perp}$ value of the o-GNPs/PLA composites with 30 wt% GNPs is 0.76 $W{\cdot}m^{-1}{\cdot}K^{-1}$. This is because that there are many gaps and defects between the 3D printed filaments in the cross-plane direction of the o-GNPs/PLA composites, leading to lots of interfacial thermal barrier in the process of phonon transmission (Fig. 2d). Therefore, the GNPs-GNPs thermally conductive pathway in the cross-plane direction of the o-GNPs/PLA composites is less efficient than that inner r-GNPs/PLA composites. As a result, the $\lambda_{\perp}$ values of the o-GNPs/PLA composites are significantly lower than those of the r-GNPs/PLA composites.

Considering from aspects of the thermal conductivities, tensile strength (Fig. S2 in ESI), storage modulus and loss modulus (Fig. S3 in ESI), and the corresponding rheological properties (Fig. S4 in ESI, processability), the optimal content of o-GNPs inner o-GNPs/PLA composites is chosen to be 20 wt%, with the related $\lambda_{\parallel}$, $\lambda_{\perp}$, tensile strength and MVR values are 2.90 $W{\cdot}m^{-1}{\cdot}K^{-1}$, 0.75 $W{\cdot}m^{-1}{\cdot}K^{-1}$, 47.5 MPa, and 13 cm^3/(10 min), respectively.

Structure and Morphologies of $Ti_3C_2T_x$ Film

The compact layered structure of Ti_3AlC_2 is shown in Fig. 3(a), while $Ti_3C_2T_x$ nanosheets present a typical two-dimensional (2D) lamellar structure with more uniform thickness (Fig. 3b). $Ti_3C_2T_x$ nanosheets have regular shape and few defects from AFM image (Fig. 3c). The correponding radial dimension is about 600 nm and the average thickness is only 2.038 nm. Fig. 3(d) shows the XRD patterns of Ti_3AlC_2 and $Ti_3C_2T_x$, which indicates that the diffraction peak at 39° corrosponding to the (104) plane disappear after acid etching. The presence of sharp diffraction

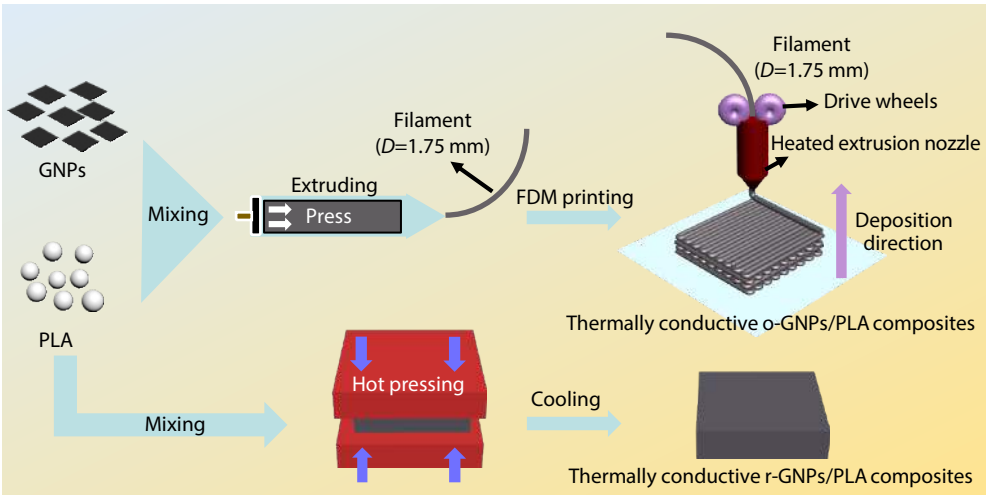

Fig. 1 Schematic illustration of the fabrication for thermally conductive GNPs/PLA composites.

https://doi.org/10.1007/s10118-022-2673-9

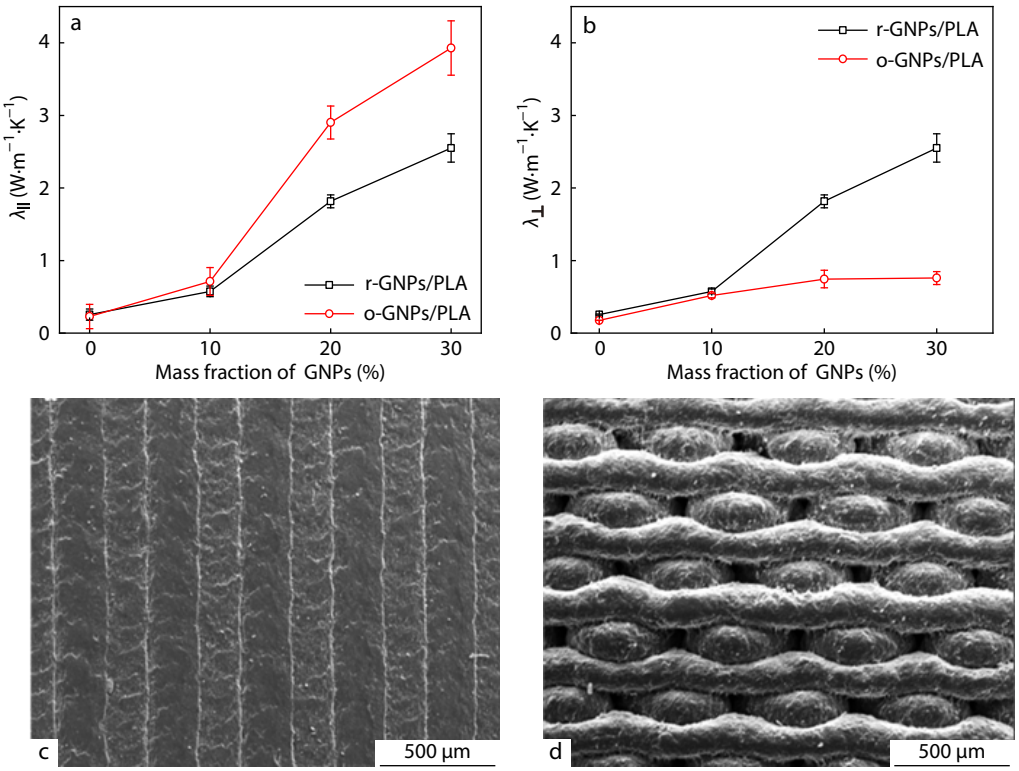

Fig. 2 $\lambda_{\parallel}$ (a) and $\lambda_{\perp}$ (b) values of the thermally conductive GNPs/PLA composites, the in-plane (c) and cross-plane (d) cross-section SEM images of 20 wt% o-GNPs/PLA composites.

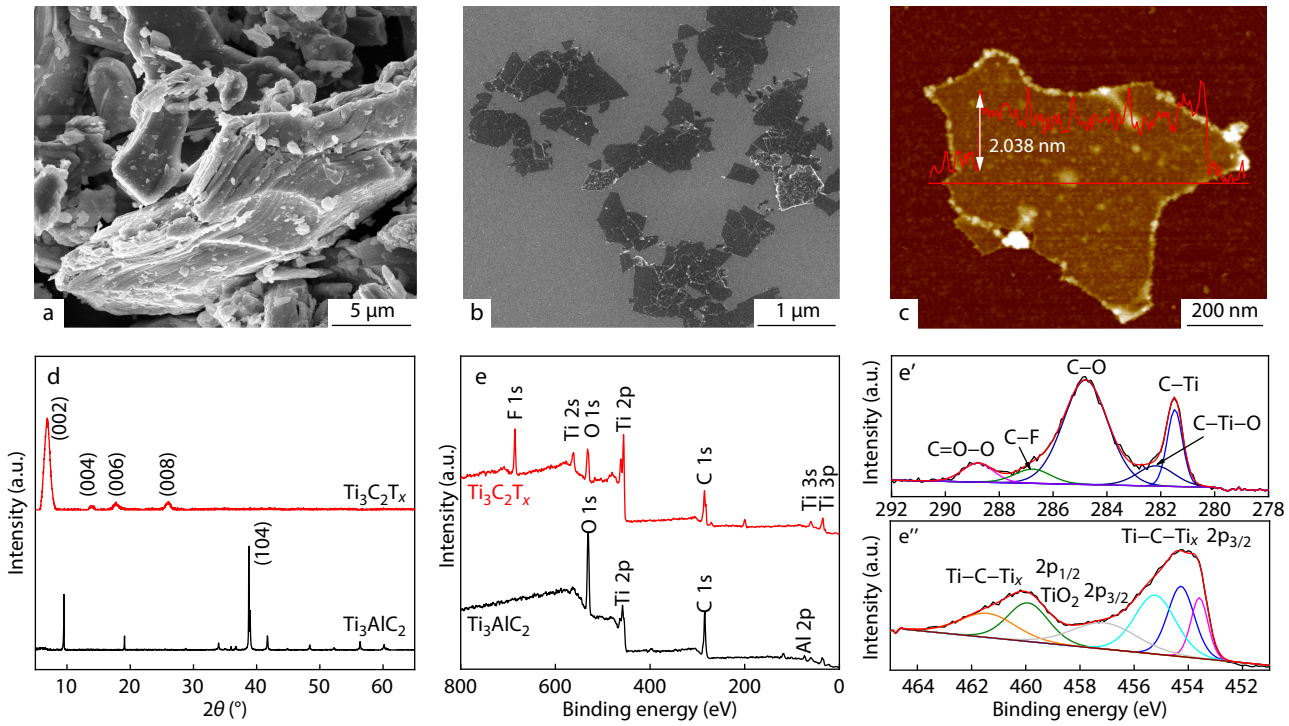

Fig. 3 SEM images of Ti_3AlC_2 (a) and $Ti_3C_2T_x$ (b); AFM image of $Ti_3C_2T_x$ (c); XRD patterns of Ti_3AlC_2 and $Ti_3C_2T_x$ (d); XPS spectra of Ti_3AlC_2 and $Ti_3C_2T_x$ (e); C 1s XPS spectrum (e′) and Ti 2p XPS spectrum (e″) of $Ti_3C_2T_x$.

peak at 6.85° and the weaker diffraction peaks at 13.78°, 17.73° and 26.10° of $Ti_3C_2T_x$ nanosheets, are attributed to the (002), (004), (006) and (008) planes, respectively. Fig. 3(e) shows the XPS full spectra of Ti_3AlC_2 and $Ti_3C_2T_x$. Ti_3AlC_2 mainly contains O,

https://doi.org/10.1007/s10118-022-2673-9

Ti, C and Al elements, while $Ti_3C_2T_x$ mainly contains F, Ti, O and C elements. For $Ti_3C_2T_x$, the characteristic peaks at 287, 531 and 685 eV correspond to C 1s, O 1s and F 1s, respectively. Peaks at 35, 60, 457 and 563 eV correspond to the characteristic peaks of Ti 3p, Ti 3s, Ti 2p and Ti 2s, respectively which indicates that Al element disappears and F element appears by strong acid etching. In addition, the surface of $Ti_3C_2T_x$ contains —OH, —F functional groups, which indicates the formation of $Ti_3C_2T_x$. Figs. 3(e′) and 3(e″) present the high resolution C 1s and Ti 2p spectra of $Ti_3C_2T_x$, repectively. Peaks at 281.5, 282.2, 284.8, 286.8 and 288.8 eV shown in Fig. 3(e′) correspond to Ti—C, C—Ti—O, C—O, C—F and O—C=O, respectively. Characteristic peak at 457.4 eV in Fig. 3(e″) corresponds to Ti=O ($2p_{3/2}$), indicating that a small amount of $Ti_3C_2T_x$ has been oxidized to TiO_2 during the reaction.[55] The above analyses demonstrate that the strong acid successfully strips Al atoms to form few-layer $Ti_3C_2T_x$.

Thermally Conductive $Ti_3C_2T_x$/(o-GNPs/PLA) Composites

Fig. 4 shows the $\lambda_{\parallel}$ and $\lambda_{\perp}$ (a) values of the thermally conductive o-GNPs/PLA and $Ti_3C_2T_x$/(o-GNPs/PLA) composites, the SEM images (b–e) of the cross section for $Ti_3C_2T_x$/(o-GNPs/PLA) composites and the EDS mapping (b′–e′) of the titanium element. As shown in Fig. 4(a), the $\lambda_{\parallel}$ and $\lambda_{\perp}$ values of the $Ti_3C_2T_x$-0/(o-GNPs/PLA) composites are 3.40 $W{\cdot}m^{-1}{\cdot}K^{-1}$ and 0.80 $W{\cdot}m^{-1}{\cdot}K^{-1}$, respectively, higher than $\lambda_{\parallel}$ (2.90 $W{\cdot}m^{-1}{\cdot}K^{-1}$) and $\lambda_{\perp}$ (0.75 $W{\cdot}m^{-1}{\cdot}K^{-1}$) of the o-GNPs/PLA composites. It is mainly due to the existence of many voids in the cross section of the o-GNPs/PLA composites by FDM 3D printing without hot pressing (Fig. S5a in ESI). The orientation of GNPs caused by FDM 3D printing process is retained inner $Ti_3C_2T_x$-0/(o-GNPs/PLA) composites, and the hot pressing process effectively eliminates the internal gap (Fig. S5b in ESI, the original gap is effectively closed by hot pressing), which is favoarable for the phonons transmission inner $Ti_3C_2T_x$-0/(o-GNPs/PLA composites, resulting in higher $\lambda_{\parallel}$ and $\lambda_{\perp}$ values than those of o-GNPs/PLA composites.

Meanwhile, the $\lambda_{\parallel}$ and $\lambda_{\perp}$ values of the $Ti_3C_2T_x$/(o-GNPs/PLA) composites increase slightly with the increase of the layer number of $Ti_3C_2T_x$ films. When the layer number of $Ti_3C_2T_x$ film is 4, the $\lambda_{\parallel}$ and $\lambda_{\perp}$ values of the $Ti_3C_2T_x$-4/(o-GNPs/PLA) composites are 3.44 $W{\cdot}m^{-1}{\cdot}K^{-1}$ and 0.82 $W{\cdot}m^{-1}{\cdot}K^{-1}$, respectively, almost at the same level as the $\lambda_{\parallel}$ (3.40 $W{\cdot}m^{-1}{\cdot}K^{-1}$) and $\lambda_{\perp}$ (0.80 $W{\cdot}m^{-1}{\cdot}K^{-1}$) of the $Ti_3C_2T_x$-0/(o-GNPs/PLA) composites. Although $Ti_3C_2T_x$ shows relatively higher intrinsic λ value than that of PLA matrix, the λ values of the $Ti_3C_2T_x$/(o-GNPs/PLA) composites are still mainly dominated by GNPs-GNPs thermally conductive pathway. The regular embedding of $Ti_3C_2T_x$ films (Figs. 4b–4e) does not cause negative effect on the λ values of the $Ti_3C_2T_x$/(o-GNPs/PLA) composites. In addition, there is no obvious interface separation and fracture at

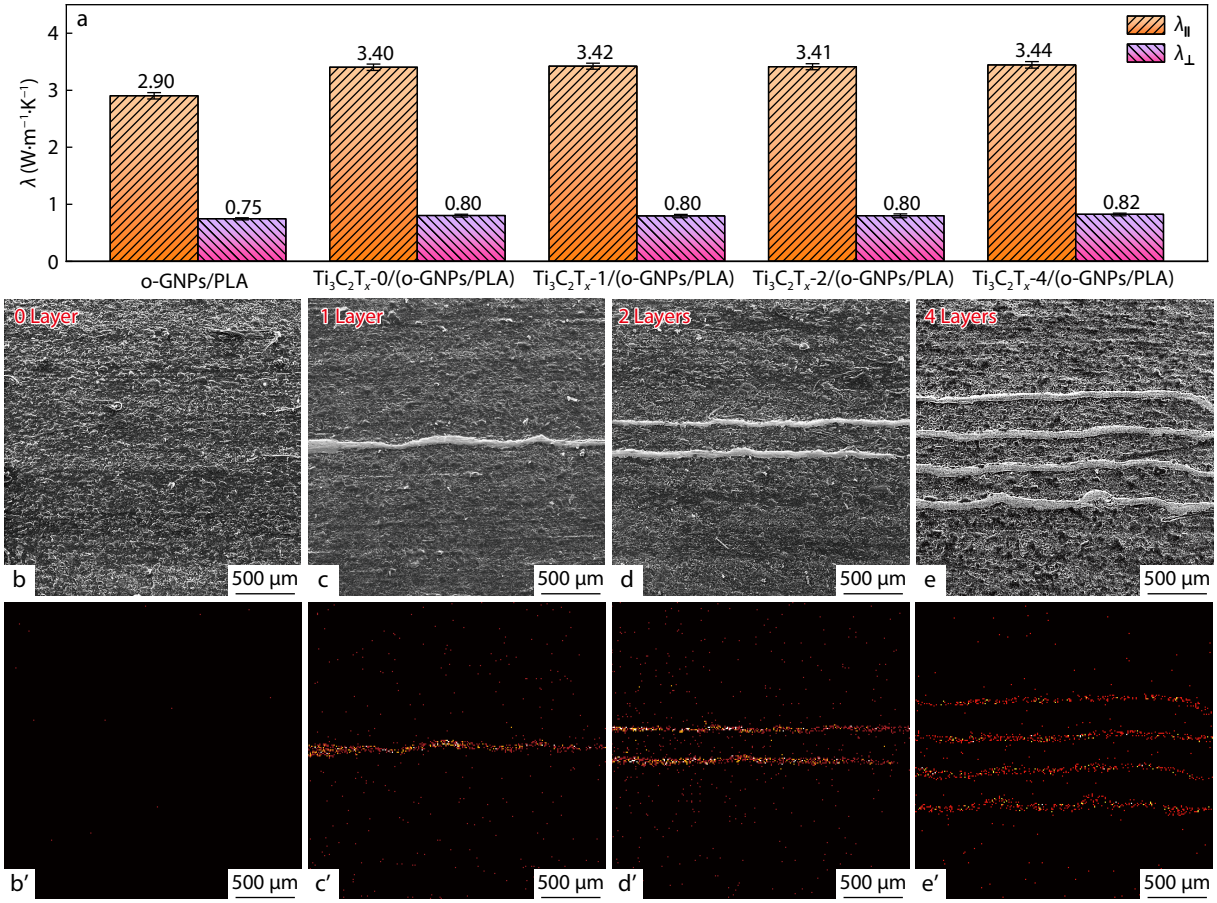

Fig. 4 $\lambda_{\parallel}$ and $\lambda_{\perp}$ values of the thermally conductive o-GNPs/PLA and $Ti_3C_2T_x$/(o-GNPs/PLA) composites (a), the corresponding cross-section SEM images (b–e) and the EDS mapping of the titanium element (b′–e′).

https://doi.org/10.1007/s10118-022-2673-9

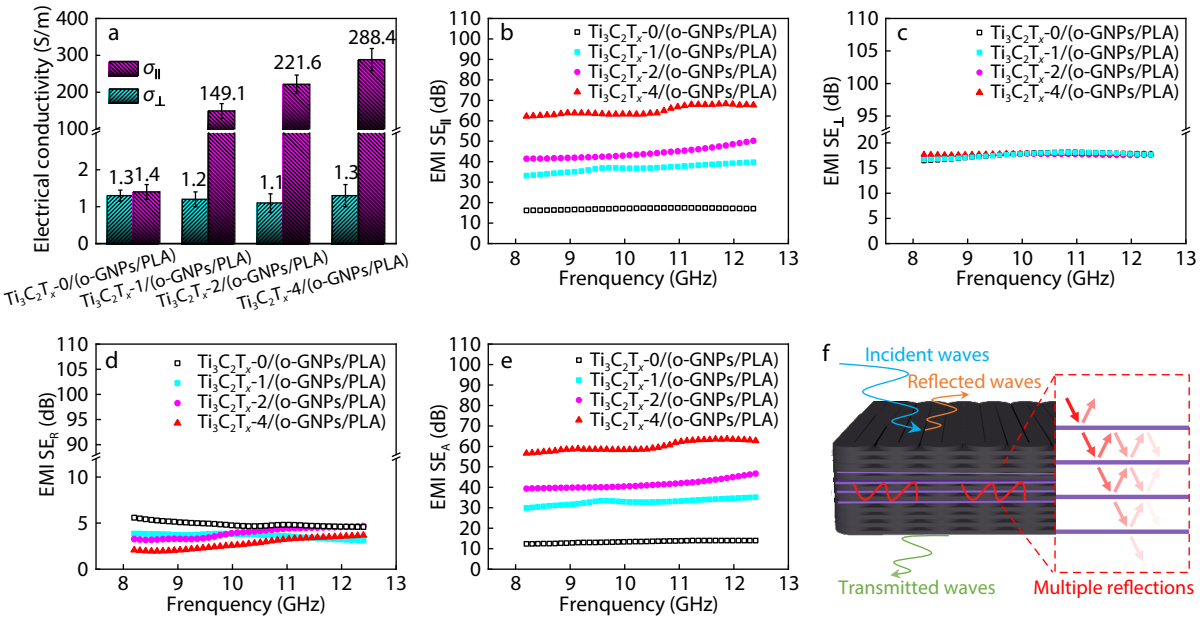

Fig. 5 σ (a), EMI SE (b–e) and schematic illustration of EMI shielding (f) for thermally conductive $Ti_3C_2T_x$/(o-GNPs/PLA) composites.

the section of the $Ti_3C_2T_x$/(o-GNPs/PLA) composites, which indictes that $Ti_3C_2T_x$ films have good interface adhesion with PLA matrix.

Fig. 5 shows the electric conductivity (σ) values of the thermally conductive $Ti_3C_2T_x$/(o-GNPs/PLA) composites (a), EMI SE (b–e) and schematic diagram (f) of electromagnetic waves passing through $Ti_3C_2T_x$/(o-GNPs/PLA) composites. With the increase of the layer number of $Ti_3C_2T_x$ films, $\sigma_{\parallel}$ and EMI $SE_{\parallel}$ values of the $Ti_3C_2T_x$/(o-GNPs/PLA) composites increase significantly, while the related $\sigma_{\perp}$ and EMI $SE_{\perp}$ values change slightly. When 4 layers of $Ti_3C_2T_x$ films are embedded, the $\sigma_{\parallel}$ and EMI $SE_{\parallel}$ values of the $Ti_3C_2T_x$-4/(o-GNPs/PLA) composites reach the maximum values of 288.4 S/m and 65 dB (at X-band), 206.0 times and 3.8 times of $\sigma_{\parallel}$ (1.4 S/m) and EMI $SE_{\parallel}$ (17 dB) values of the o-GNPs/PLA composites, respectively. While $\sigma_{\perp}$ and EMI $SE_{\perp}$ values of the $Ti_3C_2T_x$-4/(o-GNPs/PLA) composites are only 1.3 S/m and 18 dB, which are at the similar level to the $\sigma_{\perp}$ (1.3 S/m) and EMI $SE_{\perp}$ (18 dB) values of the $Ti_3C_2T_x$-0/(o-GNPs/PLA) composites. This is because when electrons transfer in the in-plane direction of the $Ti_3C_2T_x$/(o-GNPs/PLA) composites, highly conductive $Ti_3C_2T_x$ films provide more rapid transmission channels for electron transmission, resluting in significant increase of $\sigma_{\parallel}$ and EMI $SE_{\parallel}$ values. While electrons are transferred in the cross-plane direction of the $Ti_3C_2T_x$/(o-GNPs/PLA) composites, highly conductive $Ti_3C_2T_x$ films are separated by o-GNPs/PLA sheets. Therefore, the effectiveness of $Ti_3C_2T_x$ films on electron transport is not obvious, resulting in little change in $\sigma_{\perp}$ and EMI $SE_{\perp}$ values.

With the increase of the layer number of $Ti_3C_2T_x$ films, the absorption part of EMI $SE_{\parallel}$ (SE_A) of the $Ti_3C_2T_x$/(o-GNPs/PLA) composites gradually increases, while the reflection part of EMI $SE_{\parallel}$ (SE_R) changes little. When the layer number of $Ti_3C_2T_x$ films is 4, the SE_A value of the $Ti_3C_2T_x$-4/(o-GNPs/PLA) composites is 60 dB, while the SE_R is only 5 dB. This is because the microstructures inner $Ti_3C_2T_x$/(o-GNPs/PLA) composites are the stacking of o-GNPs/PLA layer and $Ti_3C_2T_x$ films layer-by-layer. The o-GNPs/PLA layers of the $Ti_3C_2T_x$/(o-GNPs/PLA) composites possess good impedance matching with the external space, resulting in a small part of incident electromagnetic waves reflected on the surface of the $Ti_3C_2T_x$/(o-GNPs/PLA) composites. After the residual electromagnetic waves are transmitted into $Ti_3C_2T_x$/(o-GNPs/PLA) composites, the multiple reflection and scattering of electromagnetic waves between "$Ti_3C_2T_x$ and o-GNPs/PLA" and "$Ti_3C_2T_x$ and $Ti_3C_2T_x$" interfaces. At the same time, the continuous $Ti_3C_2T_x$ films provide dense conductive networks. Under the action of alternating electromagnetic field, the electric charges accumulate inner $Ti_3C_2T_x$ films and generate induced current, causing conductivity loss, leading to conversion of electromagnetic energy into heat energy and the attenuation of electromagnetic waves.

CONCLUSIONS

Thermally conductive $Ti_3C_2T_x$/(o-GNPs/PLA) composites were successfully prepared by combining FDM 3D printing, vacuum assisted filtration and "layer-by-layer stacking-hot pressing" process, which achieved the construction of both phonon and electron dual transmission channels. Microstructures of $Ti_3C_2T_x$/(o-GNPs/PLA) contribute to the synergistic and efficient improvement of λ and EMI SE values of the thermally conductive $Ti_3C_2T_x$/(o-GNPs/PLA) composites. When the content of GNPs was 18.60 wt% and 4 layers of $Ti_3C_2T_x$ (6.98 wt%) films were embedded, the $\lambda_{\parallel}$ and EMI $SE_{\parallel}$ values of the thermally conductive $Ti_3C_2T_x$-4/(o-GNPs/PLA) composites increased to be 3.44 $W \cdot m^{-1} \cdot K^{-1}$ and 65 dB, which were 1223.1% and 2066.7% higher than those of neat PLA (0.26 $W \cdot m^{-1} \cdot K^{-1}$ and 3 dB). This work offers a novel and easy route for designing and manufacturing highly thermally conductive polymer composites with superior EMI SE for broader application.

https://doi.org/10.1007/s10118-022-2673-9

NOTES

The authors declare no competing financial interest.

Electronic Supplementary Information

Electronic supplementary information (ESI) is available free of charge in the online version of this article at http://doi.org/10.1007/s10118-022-2673-9.

ACKNOWLEDGMENTS

The authors are grateful for the financial support from the National Natural Science Foundation of China (Nos. 51773169 and 51973173); Technical Basis Scientific Research Project (Highly Thermally Conductive Non-metal Materials); Guangdong Basic and Applied Basic Research Foundation (No. 2019B1515120093); Natural Science Basic Research Plan for Distinguished Young Scholars in Shaanxi Province of China (No. 2019JC-11). This work was also financially supported by Polymer Electromagnetic Functional Materials Innovation Team of Shaanxi Sanqin Scholars.

REFERENCES

1 Cui, S.; Song, N.; Shi, L.; Ding, P. Enhanced thermal conductivity of bioinspired nanofibrillated cellulose hybrid films based on graphene sheets and nanodiamonds. *ACS Sustain. Chem. Eng.* **2020**, *8*, 6363–6370.
2 Yan, Q.; Dai, W.; Gao, J.; Tan, X.; Lv, L.; Ying, J.; Lu, X.; Lu, J.; Yao, Y.; Wei, Q.; Sun, R.; Yu, J.; Jiang, N.; Chen, D.; Wong, C. P.; Xiang, R.; Maruyama, S.; Lin, C. T. Ultrahigh-aspect-ratio boron nitride nanosheets leading to superhigh in-plane thermal conductivity of foldable heat spreader. *ACS Nano* **2021**, *15*, 6489–6498.
3 Wang, C.; Murugadoss, V.; Kong, J.; He, Z.; Mai, X.; Shao, Q.; Chen, Y.; Guo, L.; Liu, C. T.; Angaiahd, S.; Guo, Z. H. Overview of carbon nanostructures and nanocomposites for electromagnetic wave shielding. *Carbon* **2018**, *140*, 696–733.
4 Yun, T.; Kim, H.; Iqbal, A.; Cho, Y. S.; Lee, G. S.; Kim, M. K.; Kim, S. J.; Kim, D.; Gogotsi, Y.; Kim, S. O.; Koo, C. M. Electromagnetic interference shielding: electromagnetic shielding of monolayer MXene assemblies. *Adv. Mater.* **2020**, *32*, 2070064.
5 Song, P.; Liu, B.; Liang, C. B.; Ruan, K. P.; Qiu, H.; Ma, Z. L.; Guo, Y. Q.; Gu, J. W. Lightweight, flexible cellulose-derived carbon aerogel@reduced graphene oxide/PDMS composites with outstanding emi shielding performances and excellent thermal conductivities. *Nano-Micro Lett.* **2021**, *13*, 91.
6 Jia, Y.; Ajayi, T. D.; Wahls, B. H.; Ramakrishnan, K. R.; Ekkad, S.; Xu, C. Multifunctional ceramic composite system for simultaneous thermal protection and electromagnetic interference shielding for carbon fiber-reinforced polymer composites. *ACS Appl. Mater. Interfaces.* **2020**, *12*, 58005–58017.
7 Li, J.; Zhao, X.; Wu, W.; Ji, X.; Lu, Y.; Zhang, L. Bubble-templated rGO-graphene nanoplatelet foams encapsulated in silicon rubber for electromagnetic interference shielding and high thermal conductivity. *Chem. Eng. J.* **2021**, *415*, 129054.
8 Vu, M. C.; Choi, W. K.; Lee, S. G.; Park, P. J.; Kim, D. H.; Islam, M. A.; Kim, S. R. High thermal conductivity enhancement of polymer composites with vertically aligned silicon carbide sheet scaffolds. *ACS Appl. Mater. Interfaces* **2020**, *12*, 23388–23398.
9 Song, J. N.; Peng, Z. L.; Zhang, Y. Enhancement of thermal conductivity and mechanical properties of silicone rubber composites by using acrylate grafted siloxane copolymers. *Chem. Eng. J.* **2020**, *391*, 123476.
10 Lule, Z.; Kim, J. Thermally conductive and highly rigid polylactic acid (PLA) hybrid composite filled with surface treated alumina/nano-sized aluminum nitride. *Compos. Part A-Appl. S* **2019**, *124*, 105506.
11 Ma, T. B.; Zhao, Y. S.; Ruan, K. P.; Liu, X. R.; Zhang, J. L.; Guo, Y. Q.; Yang, X. T.; Kong, J.; Gu, J. W. Highly thermal conductivities. excellent mechanical robustness and flexibility. and outstanding thermal stabilities of aramid nanofiber composite papers with nacre-mimetic layered structures. *ACS Appl. Mater. Interfaces* **2020**, *12*, 1677–1686.
12 Yang, G.; Zhang, X. D.; Shang, Y.; Xu, P. H.; Pan, D.; Su, F. M.; Ji, Y. X.; Feng, Y. Z.; Liu, Y. Z.; Liu, C. T. Highly thermally conductive polyvinyl alcohol/boron nitride nanocomposites with interconnection oriented boron nitride nanoplatelets. *Compos. Sci. Technol.* **2021**, *201*, 108521.
13 Wu, F. P.; Lin, Z. Q.; Xu, T.; Chen, J. Y.; Huang, G. S.; Wu, H. J.; Zhou, X. Q.; Wang, D. J.; Liu, Y. F.; Hu, J. Q. Development and thermal properties of a novel sodium acetate trihydrate-acetamide-micron/nano aluminum nitride composite phase change material. *Mater. Design* **2020**, *196*, 109113.
14 Lee, W.; Kim, J. Enhanced through-plane thermal conductivity of paper-like cellulose film with treated hybrid fillers comprising boron nitride and aluminum nitride. *Compos. Sci. Technol.* **2020**, *200*, 108424.
15 Cheng, S. S.; Duan, X. Y.; Liu, X. Q.; Zhang, Z. Y.; An, D.; Zhao, G. Z.; Liu, Y. Q. Achieving significant thermal conductivity improvement *via* constructing vertically arranged and covalently bonded silicon carbide nanowires/natural rubber composites. *J. Mater. Chem. C* **2021**, *9*, 7127–7141.
16 Yao, Y. M.; Zeng, X. L.; Pan, G. R.; Sun, J. J.; Hu, J. T.; Huang, Y.; Sun, R.; Xu, J. B.; Wong, C. P. Interfacial engineering of silicon carbide nanowire/cellulose microcrystal paper toward high thermal conductivity. *ACS Appl. Mater. Interfaces* **2016**, *8*, 31248–31255.
17 Tang, X. H.; Tang, Y.; Wang, Y.; Weng ,Y. X.; Wang, M. Interfacial metallization in segregated poly(lactic acid)/poly(ε-caprolactone)/multi-walled carbon nanotubes composites for enhancing electromagnetic interference shielding. *Compos. Part A-Appl. S* **2020**, *139*, 106116.
18 Jiang, C.; Tan, D.; Li, Q.; Huang, J.; Bu, J.; Zang, L.; Ji, R. N.; Bi, S.; Guo, Q. L. High-performance and reliable silver nanotube networks for efficient and large-scale transparent electromagnetic interference shielding. *ACS Appl. Mater. Interfaces* **2021**, *13*, 15525–15535.
19 Feng, M.; Pan, Y.; Zhang, M.; Gao, Q.; Liu, C.; Shen, C.; Liu, X. H. Largely improved thermal conductivity of HDPE composites by building a 3D hybrid fillers network. *Compos. Sci. Technol.* **2021**, *206*, 108666.
20 Zhou, X.; Deng, J. R.; Fang, C. Q.; Lei, W. Q.; Song, Y. H.; Zhang, Z. S.; Huang, Z. G.; Li, Y. Additive manufacturing of CNTs/PLA composites and the correlation between microstructure and functional properties. *J. Mater. Sci. Technol.* **2021**, *60*, 27–34.
21 Mirkhani, S. A.; Iqbal, A.; Kwon, T.; Chae, A.; Kim, D.; Kim, H.; Kim, S. J.; Kim, M. K.; Koo, C. M. Reduction of electrochemically exfoliated graphene films for high-performance electromagnetic interference shielding. *ACS Appl. Mater. Interfaces* **2021**, *13*, 15827–15836.
22 Gao, M.; Peng, K.; Pan, T.; Long, F.; Lin, Y. Improving the local thermal conductivity of flexible films by microchannels filled with graphene. *Compos. Commun.* **2021**, *25*, 100689.
23 Afroj, S.; Tan, S.; Abdelkader, A. M.; Novoselov, K. S.; Karim, N. Highly conductive. scalable. and machine washable graphene-based e-textiles for multifunctional wearable electronic applications. *Adv. Funct. Mater.* **2020**, *30*, 2000293.
24 Chen, K. Y.; Gupta, S.; Tai, N. H. Reduced graphene oxide/Fe_2O_3 hollow microspheres coated sponges for flexible electromagnetic interference shielding composites. *Compos. Commun.* **2021**, *23*, 100572.
25 Agarwal, V.; Fadil, Y.; Wan, A.; Maslekar, N.; Tran, B. N.; Mat Noor, R. A.; Bhattacharyya, S.; Biazik, J.; Lim, S.; Zetterlund, P. B. Influence of anionic surfactants on the fundamental properties of

polymer/reduced graphene oxide nanocomposite films. *ACS Appl. Mater. Interfaces* **2021**, *13*, 18338–18347.
26 Pan, X. L.; Debije, M. G.; Schenning, A. P. H. J.; Bastiaansen, C. W. M. Enhanced thermal conductivity in oriented polyvinyl alcohol/graphene oxide composites. *ACS Appl. Mater. Interfaces* **2021**, *13*, 28864–28869.
27 Ruan, K. P.; Guo, Y. Q.; Gu, J. W. Liquid crystalline polyimide films with high intrinsic thermal conductivities and robust toughness. *Macromolecules* **2021**, *54*, 4934–4944.
28 Zhou, H.; Deng, H.; Zhang, L.; Fu, Q. Significant enhancement of thermal conductivity in polymer composite *via* constructing macroscopic segregated filler networks. *ACS Appl. Mater. Interfaces* **2017**, *9*, 29071–29081.
29 Ma, J. K.; Shang, T. Y.; Ren, L. L.; Yao, Y. M.; Zhang, T.; Xie, J. Q.; Zhang, B. T.; Zeng, X. L.; Sun, R.; Xu, J. B.; Wong, C. P. Through-plane assembly of carbon fibers into 3D skeleton achieving enhanced thermal conductivity of a thermal interface material. *Chem. Eng. J.* **2020**, *380*, 122550.
30 Wable, V.; Biswas, P. K.; Moheimani, R.; Aliahmad, N.; Omole, P.; Siegel, A. P.; Agarwal, M.; Dalir, H. Engineering the electrospinning of MWCNTs/epoxy nanofiber scaffolds to enhance physical and mechanical properties of CFRPs. *Compos. Sci. Technol.* **2021**, *213*, 108941.
31 Hu, J. T.; Huang, Y.; Yao, Y. M.; Pan, G. R.; Sun, J. J.; Zeng, X. L.; Sun, R.; Xu, J. B.; Song, B.; Wong, C. P. Polymer composite with improved thermal conductivity by constructing a hierarchically ordered three-dimensional interconnected network of BN. *ACS Appl. Mater. Interfaces* **2017**, *9*, 13544–13553.
32 Yang, L.; Zhang, L.; Li, C. Bridging boron nitride nanosheets with oriented carbon nanotubes by electrospinning for the fabrication of thermal conductivity enhanced flexible nanocomposites. *Compos. Sci. Technol.* **2020**, *200*, 108429.
33 Yang, X. T.; Fan, S. G.; Li, Y.; Guo, Y. Q.; Ruan, K. P.; Li, Y. G.; Zhang, S. M.; Zhang, J. L.; Kong, J.; Gu, J. W. Synchronously improved electromagnetic interference shielding and thermal conductivity for epoxy nanocomposites by constructing 3D copper nanowires/thermally annealed graphene aerogel framework. *Compos. Part A-Appl. S* **2020**, *128*, 105670.
34 Gu, J. W.; Ruan, K. P. Breaking through bottlenecks for thermally conductive polymer composites: a perspective for intrinsic thermal conductivity. interfacial thermal resistance and theoretics. *Nano-Micro Lett.* **2021**, *13*, 110.
35 Guo, Y. Q.; Ruan, K. P.; Gu, J. W. Controllable thermal conductivity in composites by constructing thermal conduction networks. *Mater. Today Phys.* **2021**, *20*, 100449.
36 Guo, Y. Q.; Yang, X. T.; Ruan, K. P.; Kong, J.; Dong, M. Y.; Zhang, J. X.; Gu, J. W.; Guo, Z. H. Reduced graphene oxide heterostructured silver nanoparticles significantly enhanced thermal conductivities in hot-pressed electrospun polyimide nanocomposites. *ACS Appl. Mater. Interfaces* **2019**, *11*, 25465–25473.
37 Yang, X. T.; Guo, Y. Q.; Han, Y. X.; Li, Y.; Ma, T. B.; Chen, M. J.; Kong, J.; Zhu, J. H.; Gu, J. W. Significant improvement of thermal conductivities for BNNS/PVA composite films *via* electrospinning followed by hot-pressing technology. *Compos. Part B-Eng.* **2019**, *175*, 107070.
38 Jiang, H.; Le Barbenchon, L.; Bednarcyk, B. A.; Scarpa, F.; Chen, Y. Bioinspired multilayered cellular composites with enhanced energy absorption and shape recovery. *Addit. Manuf.* **2020**, *36*, 101430.
39 Wiese, M.; Thiede, S.; Herrmann, C. Rapid manufacturing of automotive polymer series parts: a systematic review of processes. materials and challenges. *Addit. Manuf.* **2020**, *36*, 101582.
40 Zou, M. M.; Zhang, Y.; Cai, Z. R.; Li, C. X.; Sun, Z. Y.; Yu, C. L.; Dong, Z. C.; Wu, L.; Song, Y. L. 3D printing a biomimetic bridge-arch solar evaporator for eliminating salt accumulation with desalination and agricultural applications. *Adv. Mater.* **2021**, *2021*, 2102443.
41 Bom, S.; Martins, A. M.; Ribeiro, H. M.; Marto, J. Diving into 3D (bio)printing: a revolutionary tool to customize the production of drug and cell-based systems for skin delivery. *Int. J. Pharmaceut.* **2021**, *605*, 120794.
42 Kalkal, A.; Kumar, S.; Kumar, P.; Pradhan, R.; Willander, M.; Packirisamy, G.; Kumar, S.; DharMalhotra, B. Recent advances in 3D printing technologies for wearable (bio)sensors. *Addit. Manuf.* **2021**, *46*, 102088.
43 Diederichs, E. V.; Picard, M. C.; Chang, B. P.; Misra, M.; Mielewski, D. F.; Mohanty, A. K. Strategy to improve printability of renewable resource-based engineering plastic tailored for FDM applications. *ACS Omega* **2019**, *4*, 20297–20307.
44 Peng, F.; Jiang, H.; Woods, A.; Joo, P.; Amis, E.J.; Zacharia, N.S.; Vogt, B.D. 3D printing with core-shell filaments containing high or low density polyethylene shells. *ACS Appl. Polym. Mater.* **2019**, *1*, 275–285.
45 Deng, S.; Wu, J.; Dickey, M. D.; Zhao, Q.; Xie, T. Rapid open-air digital light 3D printing of thermoplastic polymer. *Adv. Mater.* **2019**, *31*, 1903970.
46 Liu, H.; Fu, R.; Su, X.; Wu, B.; Wang, H.; Xu, Y.; Liu, X. H. Electrical insulating MXene/PDMS/BN composite with enhanced thermal conductivity for electromagnetic shielding application. *Compos. Commun.* **2021**, *23*, 100593.
47 Gnanasekaran, K.; Heijmans, T.; Van Bennekom, S.; Woldhuis, H.; Wijnia, S.; De With, G; Friedrich, H. 3D printing of CNT- and graphene-based conductive polymer nanocomposites by fused deposition modeling. *Appl. Mater. Today* **2017**, *9*, 21–28.
48 Nguyen, N.; Zhang, S.; Oluwalowo, A.; Park, J. G.; Yao, K.; Liang, R. High-performance and lightweight thermal management devices by 3D printing and assembly of continuous carbon nanotube sheets. *ACS Appl. Mater. Interfaces* **2018**, *10*, 27171–27177.
49 Guo, Y. D.; Yang, H. N.; Lin, G. P.; Jin, H. C.; Shen, X. B.; He, J.; Miao, J.Y. Thermal performance of a 3D printed lattice-structure heat sink packaging phase change material. *Chinese J. Aeronaut.* **2021**, *34*, 373–385.
50 Jing, J.; Chen, Y.; Shi, S.; Yang, L.; Lambin, P. Facile and scalable fabrication of highly thermal conductive polyethylene/graphene nanocomposites by combining solid-state shear milling and FDM 3D-printing aligning methods. *Chem. Eng. J.* **2020**, *402*, 126218.
51 Ren, W.; Zhu, H. X.; Yang, Y. Q.; Chen, Y. H.; Duan, H. J.; Zhao, G. Z.; Liu, Y. Q. Flexible and robust silver coated non-woven fabric reinforced waterborne polyurethane films for ultra-efficient electromagnetic shielding. *Compos. Part B-Eng.* **2020**, *184*, 107745.
52 Qian, K. P.; Zhou, Q. F.; Wu, H. M.; Fang, J. H.; Miao, M.; Yang, Y. H.; Cao, S. M.; Shi, L. Y.; Feng X. Carbonized cellulose microsphere@void@MXene composite films with egg-box structure for electromagnetic interference shielding. *Compos. Part A-Appl. S* **2021**, *141*, 106229.
53 Wang, L.; Ma, Z. L.; Zhang, Y. L.; Chen, L. X.; Cao, D. P.; Gu, J. W. Polymer-based EMI shielding composites with 3D conductive networks: a mini-review. *SusMat* **2021**, *1*, 413–431.
54 Wang, Y.; Fan, Z. W.; Zhang, H.; Guo, J.; Yan, D. X.; Wang, S. F.; Dai, K.; Li, Z. M. 3D-printing of segregated carbon nanotube/polylactic acid composite with enhanced electromagnetic interference shielding and mechanical performance. *Mater. Design* **2021**, *197*, 109222.
55 Zhang, Y. L.; Ruan, K. P.; Gu, J. W. Flexible sandwich-structured electromagnetic interference shielding nanocomposite films with excellent thermal conductivities. *Small* **2021**, *17*, 2101951.
56 Huang S.; Wang L.; Li Y. C.; Liang C. B.; Zhang J. L. Novel $Ti_3C_2T_x$ MXene/epoxy intumescent fire-retardant coatings for ancient wooden architectures. *J. Appl. Polym. Sci.* **2021**, *138*, 50649.

https://doi.org/10.1007/s10118-022-2673-9